Assessment of binocular fixational eye movements including cyclotorsion with split-field binocular scanning laser ophthalmoscopy

Julia Hofmann[1,2#], Lennart Domdei[1#], Stephanie Jainta[3], Wolf Harmening[1]*

[1] Rheinische Friedrich-Wilhelms-Universität Bonn, University Eye Hospital, Bonn, Germany

[2] Fraunhofer Institute for Optronics, Systems Technologies and Image Exploitations IOSB, Karlsruhe, Germany

[3] SRH University of Applied Sciences in North Rhine-Westphalia, Hamm, Germany

equal first authors

*corresponding author: wolf.harmening@ukbonn.de, ao.ukbonn.de

JH: julia.hofmann@iosb.fraunhofer.de

LD: lennart.domdei@gmail.com

SJ: Stephanie.Jainta@srh.de

Abstract

Fixational eye motion is a hallmark of human gaze behavior, yet little is known about how they interact between fellow eyes. Here, we designed, build and validated a split-field binocular scanning laser ophthalmoscope (bSLO) to record high-resolution eye motion traces from both eyes of six observers during fixation at different binocular vergence conditions. In addition to microsaccades and drift, torsional eye motion could be extracted, with a spatial measurement error of less than 1 arcmin. Microsaccades were strongly coupled between fellow eyes under all conditions. No monocular microsaccade occurred and no significant delay between microsaccades onset across fellow eyes could be detected. Cyclotorsion was also firmly coupled between both eyes, occurring typically in conjugacy, with gradual changes during drift and abrupt changes during saccades.

Keywords

Retinal imaging; Scanning laser ophthalmoscopy; Image registration; Binocular vision; Gaze behavior; Cyclotorsion

Commercial relationships disclosure:

J Hofmann, None; **L Domdei**, None; **S Jainta**, None; **W Harmening**, None.

Introduction

Seeing with two eyes, i.e. binocularity, is central to human visual processing. For instance, ocular controls of the retinal image forming process, like pupil constriction and accommodation, are highly coupled between the two eyes (Flitcroft, Judge & Morley, 1992), and ocular motor commands issued to control gaze of one eye are tightly coupled to those of the fellow eye (Tweed, 1997; Murray, Gupta, Dulaney, Garg, Shaikh & Ghasia, 2022), for example during tracking of a moving object. Less is known whether this tight coupling extends to the phases of stable fixation, where fixational eye movements (FEM) predominate (Krauskopf, Cornsweet & Riggs, 1960; Otero-Millan, Macknik & Martinez-Conde, 2014; Simon, Schulz, Rassow & Haase ,1984). For example, Krauskopf, Cornsweet, and Riggs (1960) emphasized that microsaccades occur synchronously in both eyes (Krauskopf, Cornsweet & Riggs, 1960), but this early finding is still discussed controversially (Møller, Laursen, Tygesen & Sjølie, 2002; Engbert & Kliegl, 2003; Zhou & King, 1998). Binocular eye movements in general cannot be reduced to the yoking of the eyes during saccades: vergence eye movements occur as horizontal, vertical or cyclovergence. All three movements show substantial differences in their contributions to fusion (i.e the perception of a single object; Leigh & Zee, 2006; Schor & Ciuffreda, 1983; Steinman, Steinman, & Garzia, 2000): while horizontal vergence, for example, reacts to – on large scale and fine-tuned – horizontal disparity of the object that needs to be foveated, vertical vergence reacts to vertical misalignments of the whole image of one eye relative to the other eye. Vertical eye movements are supposed to by inherently conjugate in that vertical premotor neurons simultaneously drive both eyes (McCrea, Strassman & Highstein, 1987). Torsional eye movements (cyclovergence) are also small in overall variability (about 0.10°), and are thus tightly controlled (Van Rijn, van der Steen & Collewijn, 1994). According to van Rijn et al. (1992) cyclovergence is a truly binocular process and, unlike cycloversion, requires correspondence of the images presented to the two eyes. Finally, tremor represents a small periodic eye movement (Martinez-Conde et al., 2004; Rolfs, 2009), but weather tremor is a binocularly coordinated eye movement is still discussed (Riggs & Ratliff, 1951; Spauschus et al., 1999). Very view data exist showing all binocular eye movements – systematically – during FEM.

FEM are very small in amplitude, typically just a few minutes of arc of visual angle, and are thus not trivial to observe and to measure accurately (Rucci & Victor, 2015; Rolfs,2009). To study FEM, both spatial and temporal resolution of the measurement technique needs to be high (Poletti & Rucci, 2015; Otero-Millan, Macknik, Langston & Martinez-Conde, 2013; Chung, Kumar, Li & Levi, 2015). Such techniques include invasive means by attaching mirrors or coils directly to the moving eyeball (Barlow, 1952), or non-invasive means such as pupil and Purkinje image video-tracking (Poletti & Rucci, 2015; Martinez-Conde, Otero-Millan & Macnik, 2013), and retinal tracking by scanning laser ophthalmoscopy (SLO) (Stevenson, Roorda & Kumar, 2010; Sheehy, Yang, Arathorn, Tiruveedhula, Boer & Roorda, 2012). Owing to the obvious disadvantages of invasive measurement techniques, the highest spatial precision is currently achieved by SLO (Sheehy, Yang, Arathorn, Tiruveedhula, Boer & Roorda, 2012). If combined with potent image registration tools and micro-stimulation tools, SLO-based retinal tracking can serve as a highly sensitive gaze tracker with minimal spatial distortions artifacts (Bowers, Boehm & Roorda, 2019), allowing also to directly observe the retinal location of fixation of a visual target (Stevenson, Roorda & Kumar, 2010; Vogel, Arathorn, Roorda & Parker, 2006).

In this work, we describe an improved binocular scanning laser ophthalmoscope with which fixational eye motion can be studied during binocular vision with relative ease. We measured binocular fixational eye movements in six healthy participants. Next to high-resolution measurements of binocular gaze behavior, our analysis also allowed to extract cyclotorsion, the rotation of the eyeballs around the visual axes, with high spatial resolution.

Methods

Binocular scanning laser ophthalmoscope, bSLO

A binocular scanning laser ophthalmoscope (bSLO) was developed, similar to an earlier design described by Stevenson, Sheehy and Roorda (2016), with additional functional improvements (see **Fig. 1**). Pertinent details are described here. A mirror-based (f = 300 mm) SLO with confocal detection scheme was designed in optical simulation software (Zemax Optics Studio, Zemax Germany GmbH, Munich, Germany), and optimized to allow diffraction limited lateral resolution across a 3x3 deg field of view in each eye (see spot diagrams in **Fig. 1D**). Beam folding of the afocal, 4-f telescopic front-end followed orthogonal folding rules as laid out in Gomez-Vieyra et al. to minimize system astigmatism

(Gómez-Vieyra, Dubra, Malacara-Hernández & Williams, 2009). Light source was the fiber-coupled output of a superluminescent light emitting diode with 795 nm center wavelength (~15 nm FWHM) (SLD-CS-381-HP3-SM-795-I, Superlum, Cork, Ireland). After launching a 3.6 mm-diameter collimated beam in the reflection portion of the a 50:50 beam splitter into the bSLO front-end, galvanometric (30 Hz sawtooth) and resonant (~16 kHz sinusoidal) scanning, positioned in conjugate pupil planes, produced a raster field size of 3 x 6 (vertical x horizontal) degrees of visual angle. A knife-edge mirror, placed in a retinal plane, split the rectangular raster into two square, 3 x 3 degree half-fields, which were optically relayed separately into both eyes via a lens-based Badal optometer (Range of correctible ocular defocus: +2 to -7D). The last fold mirrors before the eyes were on single-axis translation and rotational stages that could be operated electronically to correct for interpupillary distance and binocular vergence angle. Power incident at each cornea was 200 µW. The light reflected by the retina was detected in the transmitted portion of the 50:50 beam splitter in a single photomultiplier tube (H7422-50, Hamamatsu Photonics, Hamamatsu, Japan), placed behind a confocal pinhole (pinhole diameter = 50 µm, equaling 0.9 Airy disk diameters). PMT output signals were sampled at 20 MHz by a field programmable gate array (FPGA) to produce 512x512 pixel video frames at 29.3 Hz.

Eye motion extraction from bSLO videos

Due to the field-split design of the bSLO, a single video frame consisted of two half images of each retina recorded side-by-side (**Fig. 2A**). Because of the equal aspect ratio in the FPGA digital sampling and the rectangular optical scanning field with an aspect ratio of 1:2 (horizontal:vertical), retinal image space in each half-image is compressed along the horizontal dimension two-fold. This was compensated later by multiplying horizontal motion signals by 2. Binocular eye motion extraction was achieved by an offline strip-wise image registration described earlier of each half-field independently (Stevenson, Roorda & Kumar, 2010). In brief, half images were divided into 32 horizontal strips, each 16 pixels high, and registered to an automatically extracted reference frame from a longer video sequence (**Fig. 2B**). This resulted in a high-resolution eye motion trace with 960 Hz sampling frequency. From each video, horizontal and vertical motion traces of both eyes were further analyzed. In those traces, microsaccades were semi-manually labelled by first thresholding motion velocity, and then validating each candidate saccade manually (**Fig. 2C**). The onset of a

microsaccade was defined at the first sample exceeding a velocity of 0.25 arcmin/ms in a moving average of 3 data samples. In the horizontal direction, eye movements shifting gaze to the right were expressed by positive value changes. In the vertical, positive value changes mean gaze upwards (both directions in the visual field as seen from behind the participant).

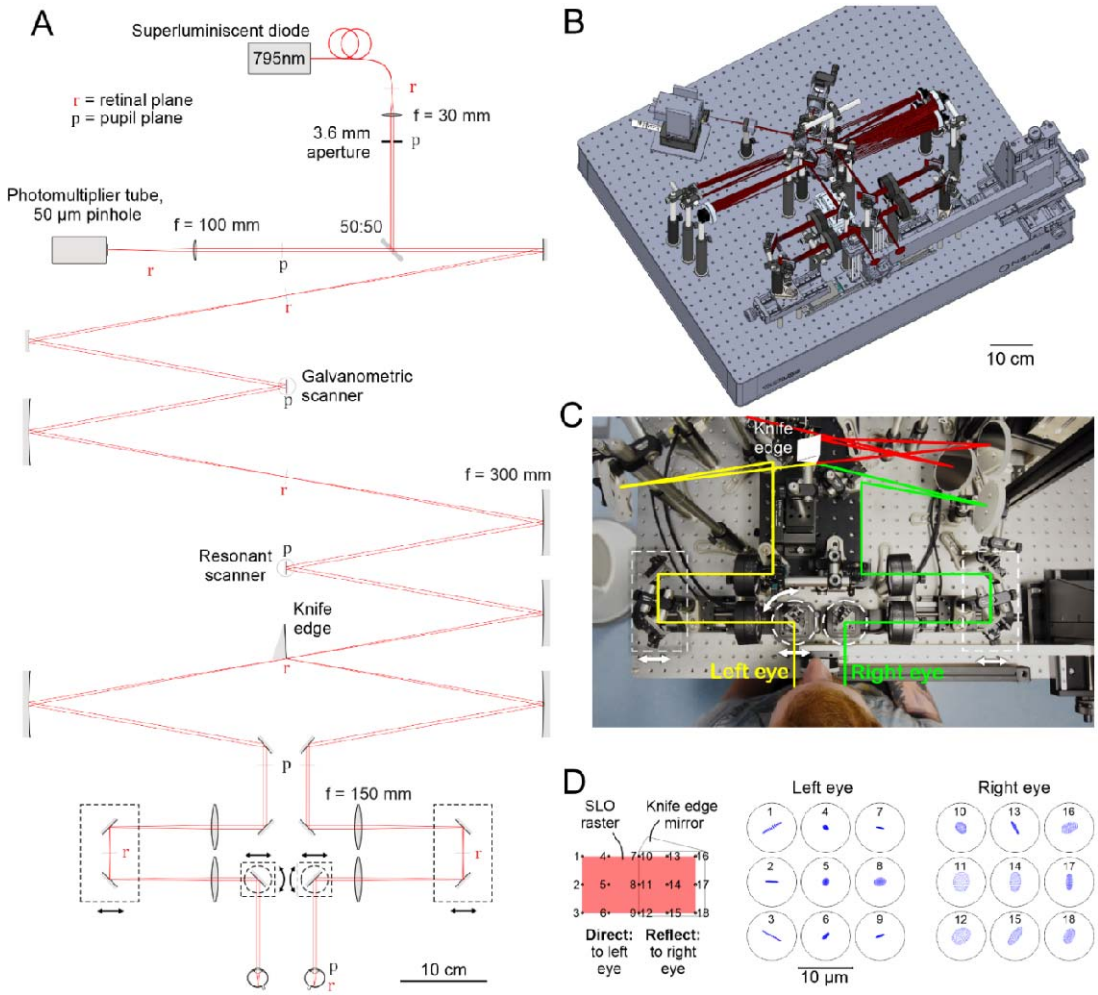

Figure 1 | Binocular scanning laser ophthalmoscope (bSLO). **A**: Schematic drawing of the bSLO setup. Components are drawn to scale; the beam path is shown unfolded for clarity (compare **B** for actual beam path). Translation and rotation stages marked by dashed lines. Scale is given along the direction of beam propagation. **B**: Three-dimensional model of the actual beam path and optomechanical components. **C**: Top view photograph of the front-end with indication of beam paths for both eyes and position of moveable stages. **D**: Simulated spot diagrams at the 18 cardinal points of the bSLO raster, spanning square imaging fields in the two eyes. Circles indicate Airy disk diameter.

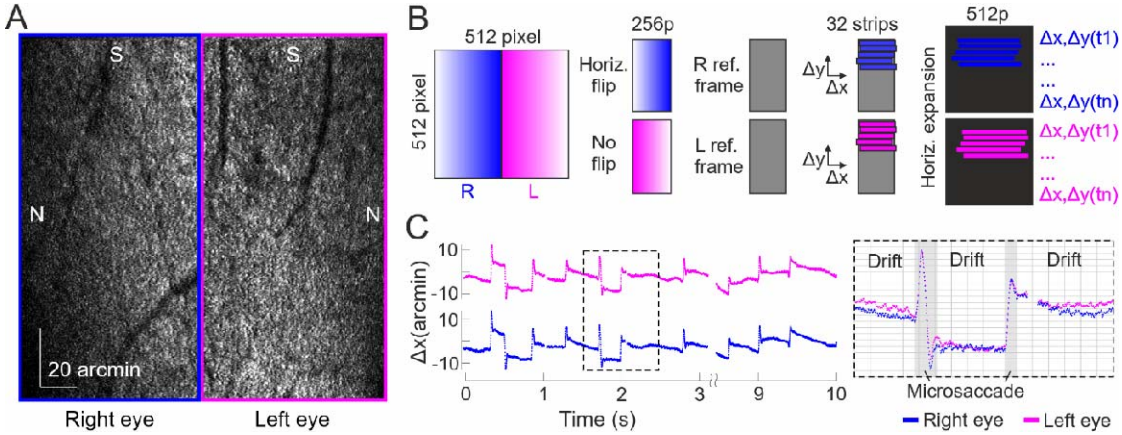

Figure 2 | Eye motion extraction from bSLO imagery. **A:** Single bSLO video frame while the participant fixated on the upper right corner of the scanning raster in both eyes. Note that the right eye's image is horizontally flipped due to the scan geometry and beam folding (S: superior, N: nasal on the retina). **B**: Half-images in single bSLO frames were separated and brought into fundus orientation before strip-wise image registration. Horizontal image shifts were multiplied by 2 to account for the unequal image aspect ratio. **C:** Example retinal motion trace of both eyes (horizontal portion only), microsaccades were detected automatically by velocity thresholding of a 7-sample moving average.

Estimation of cyclotorsional eye motion

Eye motion traces resulted from strip-wise image translations relative to a reference frame. If the acquired image is however rotated against that reference, e.g. during cyclotorsional movement of the eye, eye motion traces will contain an additional horizontal component beating at frame rate, resembling a sawtooth pattern. This particular rotational artifact is pronounced in the horizontal dimension due to the predominantly horizontal geometry of the image strips (**Fig. 3A**). We found a linear relationship between the slope at which horizontal strip offsets appeared at frame rate when the reference frame was rotated computationally in an interval between 0 and 30 arcmin and then registered to bSLO videos that contained no visible rotation artifact. 604 bSLO frames selected from different sessions and eyes were probed in this way to derive a factor of 3.77 between the measured gradient in motion traces (in arcmin per frame) and angle of image rotation (in arcmin) (**Fig. 3B**). As a result, cyclotorsion signals could be derived at frame rate in all bLSO eye motion traces. Due to the large change in slope during a microsaccade, these epochs were excluded from cyclotorsional analysis (**Fig. 3C**). Motion trace slope that was due to simultaneous drift was

separated from torsion signals. For this, the drift slope was calculated by the difference of the mean drift per frame and then subtracted from the torsion slope, leaving the isolated torsion value. Throughout this paper, positive torsional values correspond to clockwise eye rotation as seen from behind the participant.

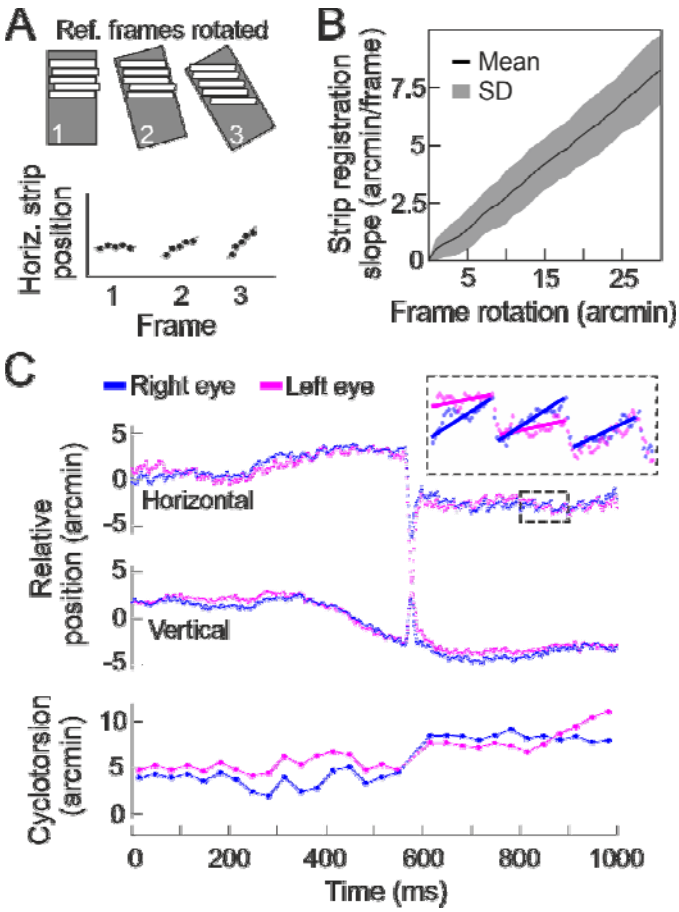

Figure 3 | **Estimation of cyclotorsional eye motion. A:** Cyclotorsion produced a sawtooth pattern beating at frame rate in horizontal eye motion traces. **B:** By computationally rotating the reference frame, a linear relationship between beat gradient and rotation angle was determined. **C:** Exemplary torsional analysis with the typical sawtooth pattern highlighted in the inset Typically, torsion changed with a microsaccade.

Assessment of binocular FEM

Binocular fixational eye movements (bFEM) were measured in six healthy volunteers (one female, five males, mean age: 34), referred to as P1 to P6 throughout the manuscript. Participant naming was based on a decreasing order of the magnitude of fixational stability,

with P1 exhibiting the lowest average binocular iso-contour areas (see **Results**). Refractive state was measured by an auto-refractor and was between -0.125 and - 3 diopters best spherical equivalent. While the participant's head was immobilized in front of the bSLO by a dental impression (bite bar) held on a XYZ-translation stage, they were asked to fixate on the top right corner of the individual scan raster seen by each eye as relaxed and accurate as possible. Binocular vergence of the last fold mirror of the bSLO was set to either 0, 1, 2, 3, 4 or 5 degrees for each video, in ascending or descending order for half of the subjects, respectively. Five ~10-second long bSLO videos were recorded at each viewing condition (one video comprised 300 frames = 10.24 s). Pupils were dilated by instilling one drop of 1 % Tropicamide 15 minutes before the beginning of the recording session. Written informed consent was obtained from each participant and all experimental procedures adhered to the tenets of the Declaration of Helsinki, in accordance with the guidelines of the independent ethics committee of the medical faculty at the Rheinische Friedrich-Wilhelms-Universität of Bonn, Germany.

Results

Binocular coordination of fixational eye movements

In all six participants (P1-P6), binocular FEM were derived from thirty ~10-second videos during six different binocular vergence angles (5 in each condition). In each video, horizontal and vertical movements of both eyes were extracted at 960 Hz, torsion was extracted at 30 Hz (see Methods). After removing video frames containing eye blinks and frames that could not be registered to the reference frame (due to out of field motion and other registration errors), we arrived at a total of 1,564,640 samples collected for transversal movement for all eyes combined, and after an additional exclusion of microsaccade epochs, at a total of 37,228 samples for torsional movement. Relative vergence and version were computed by subtracting or averaging the left and right eye motion traces, respectively (an example data set is shown in **Fig. 4** of P4 at a vergence angle of 2° degree).

In general, binocular eye coordination was high for all subjects across all conditions. The average vergence motion (computed as L-R position signals) was 1.18 arcmin (standard deviation, SD: 1.21 arcmin) in the horizontal, and 0.56 arcmin (SD: 0.53 arcmin) in the vertical direction. Within 4,052 total microsaccades detected across all subjects, we did not

observe a monocular microsaccade, i.e. one that is present only in one eye. Microsaccade frequency varied across participants (average microsaccades per second, P1: 1.12, P2: 0.71, P3: 0.62, P4: 1.68, P5: 1.41). Temporal microsaccade onset difference between eyes was distributed normally around an average of 1.03 ms (SD: 1.23 ms). The main sequence of microsaccades, defined as the relationship between peak velocity and excursion amplitude showed a typical linear relationship in log-log plotting, with an average slope of 0.073 ms^{-1} across eyes, equal for fellow eyes (Pearson's correlation between the left and right eye >0.99 for all subjects). Microsaccade amplitude and direction were firmly coupled between the two eyes (average amplitude deviance = 1.34 arcmin, SD: 1.88 arcmin, average direction deviance = 0.52 arcmin, std: 0.72 arcmin).

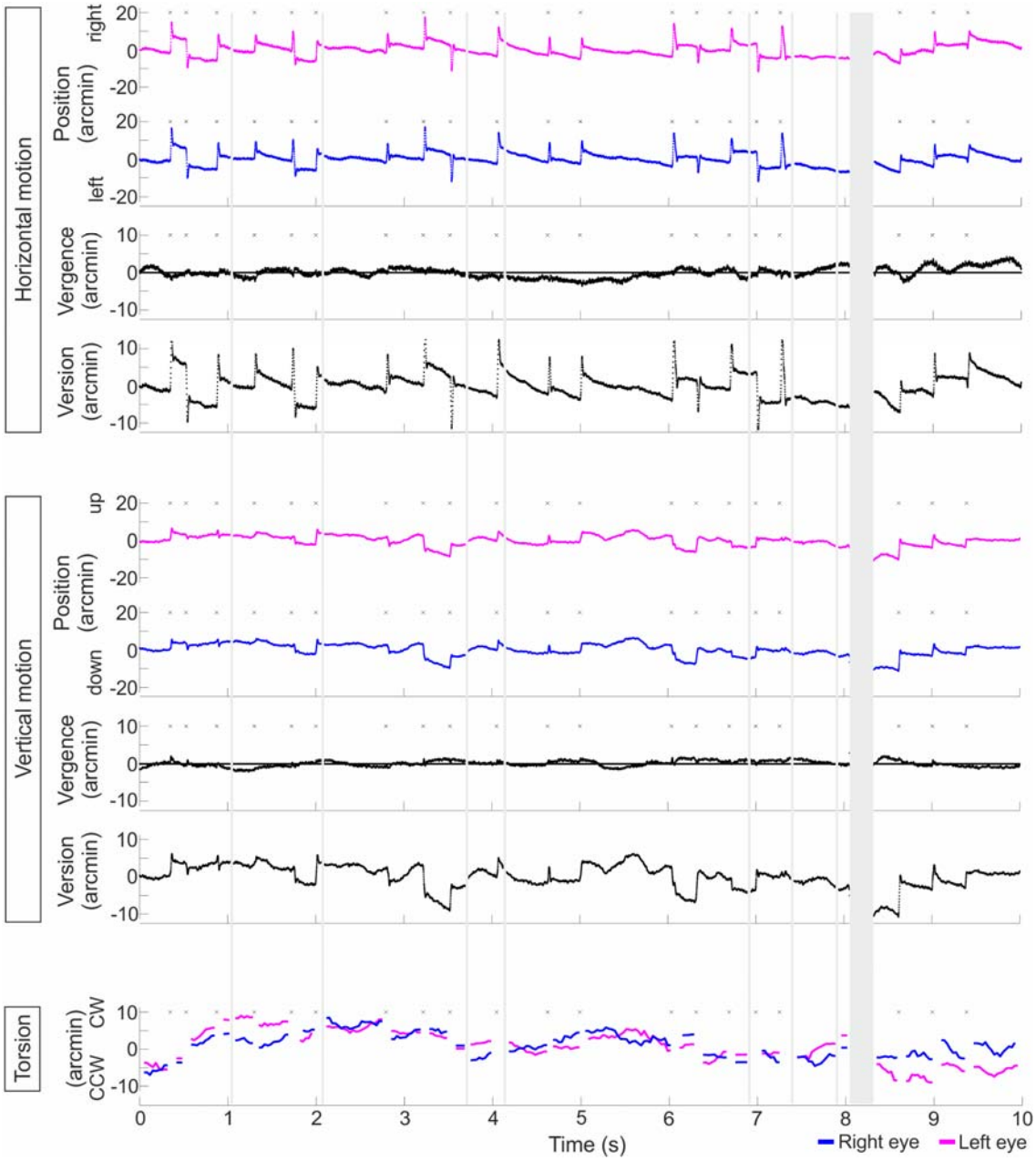

Figure 4 | **Exemplary binocular eye motion traces**. Data is from a single 10-second video recorded in P6 at two deg vergence angle. Ten of such videos were recorded per viewing condition per participant. Colors indicate fellow eyes (left = magenta, right = blue). Horizontal, vertical and torsional movements are shown separately. Small asterisks indicate the occurrence of a microsaccade for which torsion was undefined.

In an analysis of fixation stability, expressing all retinal landing points of the fixated object in a two-dimensional plot as their iso-contour area (ISOA, encompassing 68% of all data points), a corresponding relationship emerged (**Fig. 5**). While the magnitude of ISOAs differed between participants (average ISOA: P1: 15.62 $arcmin^2$, P2: 24.97 $arcmin^2$, P3: 27.04 $arcmin^2$, P4: 28.46 $arcmin^2$, P5: 29.57 $arcmin^2$, P6: 31.02 $arcmin^2$), fellow-eye ISOAs were similar (Pearson's correlation between ISOAs of the left and right eye for each participant: P1: ρ=0.78, P2: ρ=0.84, P3: ρ=0.79, P4: ρ=0.62, P5: ρ=0.61, P6: ρ=0.96, all $p<<0.01$). ISOAs of binocular data points (L-R) were always smaller than monocular ISOAs (average: 3.48 to 8.04 $arcmin^2$, P1 to P6, respectively, average range of monoISOA:binoISOA = 4,52 at binocular vergence of 0°). Binocular ISOAs, unlike monocular ISOAs, were elongated in the horizontal direction, being on average 2.2 times wider than high. We observed a weak yet insignificant trend of increasing monocular ISOAs with larger vergence angles set in the bSLO. However, binocular coupling did not seem to be systematically disturbed by the vergence induced. In all participants, and across all vergence angles, binocular fixation stability (L-R) was always lower then monocular fixation stability (average ISOA ratio mono/bino, 0°: 4.98, 1°: 7.16, 2°: 8.29, 3°: 8.78, 4°: 7.13, 5°: 7.93).

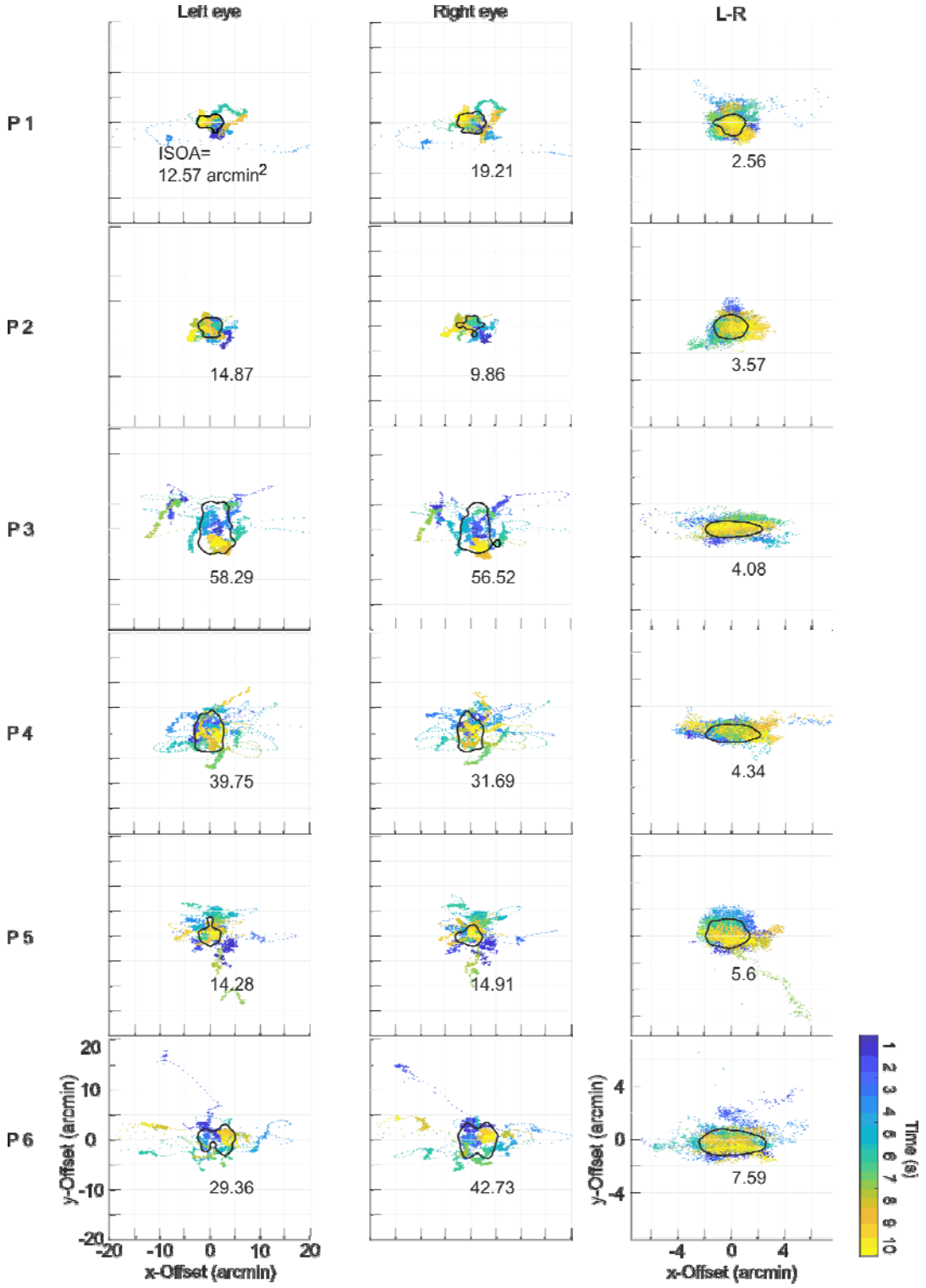

Figure 5 | **Monocular and binocular fixational stability.** Data is from one 10-second video at 0 deg vergence angle for all participants (P1-P6). Fixation target was the corner of the 3x3 degree scanning raster. Time is color coded. The ISOAs (black outline) are given in arcmin^2. Note that the scale has been magnified for the binocular (L-R) data set 2.5-fold.

Cyclotorsion during fixational eye motion

From the computationally rotated reference frame analysis we could derive a variance of strip offset for each rotational angle. The smallest offset which could be observed was 0.7 arcmin. The smallest torsional angle which could be measured was 0.6 arcmin. The square root of the average variance (SD: 0.47 arcmin) was multiplied by 2.77 to arrive at a repeatability of 1.3 arcmin. Measurement error was thus 0.92 arcmin (variance multiplied by 1.96). Across all eyes and viewing conditions, torsional angles between -34.0 and 34.6 arcmin were observed (average: 0.52 arcmin, std: 5.72 arcmin). Correlated to the metrics of fixations stability and frequency of microsaccades, the distribution of torsional motion was idiosyncratic across participants (**Fig. 7**). A linear fit to a correlation of left and right eyes' torsion demonstrated tight coupling (mean slope = 1.05, sigma^2 = 0.0005).

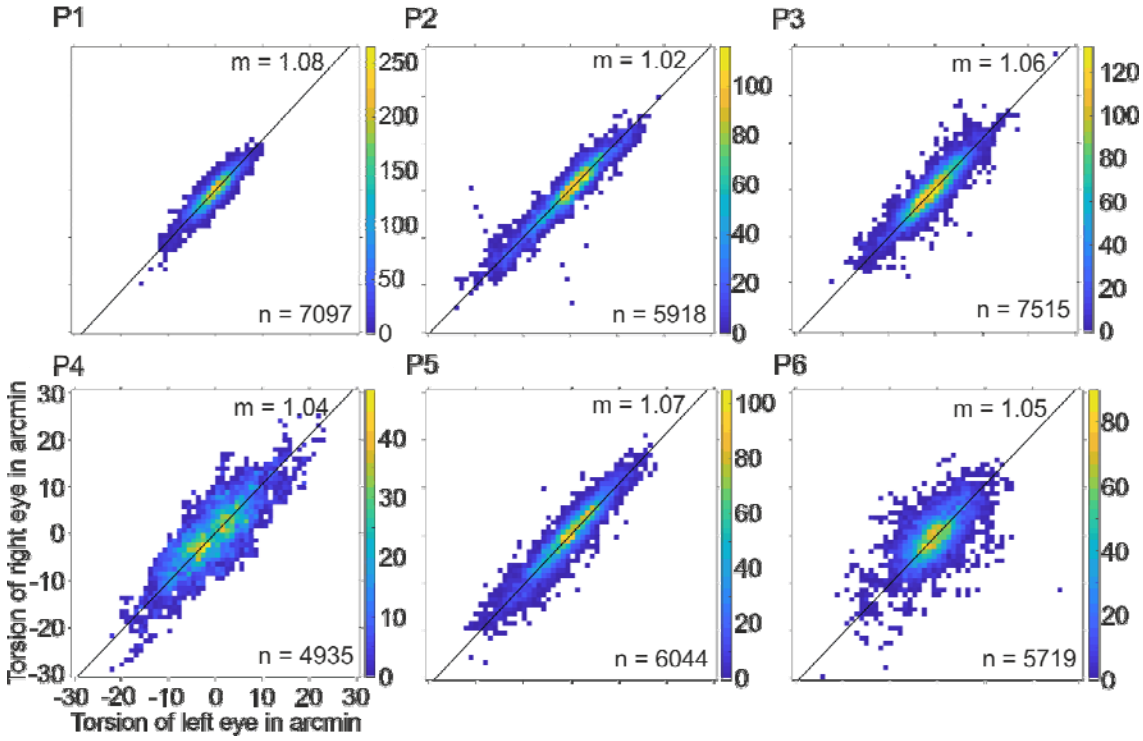

Figure 7| Point-wise correlation of fixational cyclotorsion between fellow eyes of all participants (P1-P6). Each pixel is 1 arcmin squared and color coded for the number of occurrences. N is the total numbers of observed torsion samples per participant. The solid line is the linear fit of the density map, with slope m. A slope of exactly 1 would mean a perfect correlation of the torsional motion of both eyes.

Discussion

By improving the design of a split-field binocular scanning laser ophthalmoscope, we assessed fixational eye movements including cyclotorsion in six healthy participants.

As expected, and similar to earlier monocular SLO systems, we could demonstrate high temporal (~1 kHz) and spatial resolution (~12 arcsec) for both horizontal and vertical eye motion estimation in both eyes simultaneously. Given the split-field design in our system, the right and left eye's image content is recorded quasi-simultaneously, removing the need of temporal synchronization. In reality, the right and left signals are recorded block-wise (R, L, R, L, …), with a constant temporal offset between right and left signal onsets equal to half of the line rate (~6.7 µs), which is less than 0.5% of the temporal sampling rate of about 1 ms.

In general, temporal and spatial resolution of SLO-based retinal tracking is equal or superior to commercial video based binocular eye trackers (Sheehy, Yang, Arathorn, Tiruveedhula, Boer & Roorda, 2012), but only for eye motion amplitudes that are on the order of the imaging field size. Eye motion that produces image content with insufficient overlap to a common reference frame cannot be estimated reliably with such a system (Stevenson, Roorda & Kumar, 2010). This makes SLO-based retinal tracking ideal to study fixational eye motion, given their smaller amplitude (Rolfs, 2009). If image acquisition in a retinal imager is fast enough, temporally adjacent video frames can contain sufficient spatial overlap that removes the need of a common reference frame, and thus allows out-of-field tracking (Szkulmowski et al., 2020). Such an approach may offer, on the other hand, not enough spatial resolution to resolve retinal structure of interest, which may be important if gaze behavior and retinal cell topography is wished to be linked (Reiniger, Domdei, Holz & Harmening, 2021; Ratnam, Domdei, Harmening & Roorda, 2017; Harmening, Tuten, Roorda & Sincich, 2014)

The system presented here offers some technical improvements to a similar split-field binocular SLO demonstrated earlier (Stevenson, Sheehy & Roorda, 2016). First, 3 x 3 degree imaging fields were used, accommodating larger eye movements. Typical fixational eye motion ranges from ~11-60 arcsec (Tremor) to 7.5 ± 1.5 arcmin (Microsaccades) (Bowers,

Boehm & Roorda, 2019; Montes, Bennett, Bensinger, Rani, Sherkat, Zhao & Sheehy, 2022), which would put our method in the position to cover most fixational situations. Two independent Badal optometers allowed correction of ocular lower order aberrations, the largest factor reducing image quality in ophthalmic imaging (Steven, Sulai, Cheong, Bentley & Dubra, 2018). This will allow to increase observation numbers in normal participants and patients, given that eyes do not have to be preselected based on favorable refractive states.

Interpupillary distance could be adjusted using motorized platforms, which together with an optional pupil monitor camera allowed relatively easy and quick binocular alignment. This will increase imaging and workflow efficiency by decreasing chair time.

Finally, binocular vergence angles could be independently induced by motorized rotation platforms, adding experimental options for binocular vision science experiments. Our system was built and optically optimized to accommodate a second light channel in the future for multi-wavelength binocular micro-stimulation (REF Harmening 2014).

In this work, cyclotorsional motion during fixation was extracted by analysis of the sawtooth pattern artifact in the horizontal movement track, as suggested in prior studies (Stevenson, Roorda & Kumar, 2010; Bowers, Boehm, & Roorda, 2019). After calibrating this linkage with synthetic image data (see Methods), cyclotorsional movement could be estimayed with an angular resolution of less than 1 arcmin. We note, however, that torsion signals are theoretically confounded by other artifacts in the estimated motion paths. Thus, accurate torsion estimation would benefit from distortion free reference frame generation, an ongoing topic in SLO based eye motion research (Shenoy, Fong, Tan, Roorda & Ng, 2021; Bedggood & Metha, 2017; Bedggood & Metha, 2019).

We found that torsional motion was largely coupled between the two eyes, and, in accordance with earlier work, often occurred immediately after a saccade (Murdison, Blohm & Bremmer, 2019). Thus, our data tentatively suggests that torsional eye movements correct slight misallocations of the eyes after saccades (Howard, 2012) in a conjugate fashion. As a further qualitative observation, torsional motion corresponded to horizontal and vertical movement patterns of fixational eye movements, with gradual changes during drift and abrupt changes during saccades. More data for different fixation stimuli is clearly

needed to evaluate the functional role of such fixational eye movements in respect of single eye or binocular coordinated processes, and we proved the present binocular scanning laser ophthalmoscope to be an apt setup for such research.

Conclusion

A split-field binocular scanning laser ophthalmoscope (bSLO) was designed, build and used to record high-resolution eye motion traces from both eyes of six observers at different binocular vergence conditions. In addition to microsaccades and drift, torsional eye motion could be extracted, with a spatial measurement error of less than 1 arcmin. Fixational microsaccades were strongly coupled between fellow eyes under all conditions. No monocular microsaccade occurred and no significant delay between microsaccades onset across fellow eyes could be detected. Cyclotorsion was highly coupled between both eyes.

Acknowledgements

We thank Austin Roorda and Pavan Tiruveedhula for technical resources. This study was funded by a research grant of the Dr. Eberhard and Hilde Rüdiger Stiftung (BINOSLO), and by the Emmy Noether-Program of the German Research Foundation (DFG, Ha 5323/5-1,2).

References

Barlow, H. B. (1952). Eye movements during fixation. *The Journal of Physiology*, 116(3), 290, https://doi.org/10.1113/jphysiol.1952.sp004706.

Bedggood, P., & Metha, A. (2017). De-warping of images and improved eye tracking for the scanning laser ophthalmoscope. *PloS one*, 12(4), e0174617, https://doi.org/10.1371/journal.pone.0174617.

Bedggood, P., & Metha, A. (2019). Mapping flow velocity in the human retinal capillary network with pixel intensity cross correlation. *PloS one*, 14(6), e0218918, https://doi.org/10.1371/journal.pone.0218918.

Bowers, N. R., Boehm, A. E., & Roorda, A. (2019). The effects of fixational tremor on the retinal image. *Journal of vision*, 19(11), 8-8, https://doi.org/10.1167/19.11.8.

Chung, S. T., Kumar, G., Li, R. W., & Levi, D. M. (2015). Characteristics of fixational eye movements in amblyopia: Limitations on fixation stability and acuity? *Vision research*, 114, 87-99, https://doi.org/10.1016/j.visres.2015.01.016.

Engbert, R., & Kliegl, R. (2003). Microsaccades uncover the orientation of covert attention. *Vision research*, 43(9), 1035-1045, https://doi.org/10.1016/S0042-6989(03)00084-1.

Flitcroft, D. I., Judge, S. J., & Morley, J. W. (1992). Binocular interactions in accommodation control: effects of anisometropic stimuli. *Journal of Neuroscience*, 12(1), 188-203, https://doi.org/10.1523/JNEUROSCI.12-01-00188.1992.

Gómez-Vieyra, A., Dubra, A., Malacara-Hernández, D., & Williams, D. R. (2009). First-order design of off-axis reflective ophthalmic adaptive optics systems using afocal telescopes. *Optics express*, 17(21), 18906-18919, https://doi.org/10.1364/OE.17.018906.

Harmening, W. M., Tuten, W. S., Roorda, A., & Sincich, L. C. (2014). Mapping the perceptual grain of the human retina. *Journal of Neuroscience*, 34(16), 5667-5677, https://doi.org/10.1523/JNEUROSCI.5191-13.2014.

Howard, I. P. (2012). *Perceiving in depth, volume 1: basic mechanisms*. Oxford University Press.

Ko, H. K., Poletti, M., & Rucci, M. (2010). Microsaccades precisely relocate gaze in a high visual acuity task. *Nature neuroscience*, 13(12), 1549-1553, https://doi.org/10.1038/nn.2663.

Krauskopf, J., Cornsweet, T. N., & Riggs, L. A. (1960). Analysis of eye movements during monocular and binocular fixation. *JOSA*, 50(6), 572-578, https://doi.org/10.1364/JOSA.50.000572.

Leigh, R. J., & Zee, D. S. (2006). The neurology of eye movements fourth edition. *CONTEMPORARY NEUROLOGY SERIES*, *70*(1).

Martinez-Conde, S. (2006). Fixational eye movements in normal and pathological vision. *Progress in brain research*, 154, 151-176, https://doi.org/10.1016/S0079-6123(06)54008-7.

Martinez-Conde, S., Macknik, S. L., & Hubel, D. H. (2004). The role of fixational eye movements in visual perception. *Nature reviews neuroscience*, 5(3), 229-240, https://doi.org/10.1038/nrn1348.

Martinez-Conde, S., Otero-Millan, J., & Macknik, S. L. (2013). The impact of microsaccades on vision: towards a unified theory of saccadic function. *Nature Reviews Neuroscience*, 14(2), 83-96, https://doi.org/10.1038/nrn3405.

McCrea, R. A., Strassman, A., May, E., & Highstein, S. M. (1987). Anatomical and physiological characteristics of vestibular neurons mediating the horizontal vestibulo-ocular reflex of the

squirrel monkey. *Journal of Comparative Neurology*, *264*(4), 547-570, https://doi.org/10.1002/cne.902640408.

Møller, F., Laursen, M., Tygesen, J., & Sjølie, A. (2002). Binocular quantification and characterization of microsaccades. *Graefe's archive for clinical and experimental ophthalmology*, 240(9), 765-770, https://doi.org/10.1007/S00417-002-0519-2.

Montes, S. Y. C., Bennett, D., Bensinger, E., Rani, L., Sherkat, Y., Zhao, C., ... & Sheehy, C. K. (2022). Characterizing Fixational Eye Motion Variance Over Time as Recorded by the Tracking Scanning Laser Ophthalmoscope. *Translational Vision Science & Technology*, 11(2), 35-35, https://doi.org/10.1167/tvst.11.2.35.

Murdison, T. S., Blohm, G., & Bremmer, F. (2019). Saccade-induced changes in ocular torsion reveal predictive orientation perception. *Journal of Vision*, 19(11), 10-10, https://doi.org/10.1167/19.11.10.

Murray, J., Gupta, P., Dulaney, C., Garg, K., Shaikh, A. G., & Ghasia, F. F. (2022). Effect of Viewing Conditions on Fixation Eye Movements and Eye Alignment in Amblyopia. *Investigative Ophthalmology & Visual Science*, 63(2), 33-33, https://doi.org/10.1167/iovs.63.2.33.

Otero-Millan, J., Macknik, S. L., Langston, R. E., & Martinez-Conde, S. (2013). An oculomotor continuum from exploration to fixation. *Proceedings of the National Academy of Sciences*, 110(15), 6175-6180, https://doi.org/10.1073/pnas.1222715110.

Otero-Millan, J., Macknik, S. L., & Martinez-Conde, S. (2014). Fixational eye movements and binocular vision. *Frontiers in integrative neuroscience*, 8, 52, https://doi.org/10.3389/fnint.2014.00052.

Poletti, M., Listorti, C., & Rucci, M. (2010). Stability of the visual world during eye drift. *Journal of Neuroscience*, 30(33), 11143-11150, https://doi.org/10.1523/JNEUROSCI.1925-10.2010.

Poletti, M., & Rucci, M. (2015). A compact field guide to the study of microsaccades: Challenges and functions. *Vision research*, 118, 83-97, https://doi.org/10.1016/j.visres.2015.01.018.

Ratnam, K., Domdei, N., Harmening, W. M., & Roorda, A. (2017). Benefits of retinal image motion at the limits of spatial vision. *Journal of vision*, *17*(1), 30-30, https://doi.org/10.1167/17.1.30.

Reiniger, J. L., Domdei, N., Holz, F. G., & Harmening, W. M. (2021). Human gaze is systematically offset from the center of cone topography. *Current Biology*, *31*(18), 4188-4193, https://doi.org/10.1016/j.cub.2021.07.005.

Riggs, L. A., & Ratliff, F. (1951). Visual acuity and the normal tremor of the eyes. *Science*, *114*(2949), 17-18, https://doi.org/10.1126/science.114.2949.17.

Rolfs, M. (2009). Microsaccades: small steps on a long way. *Vision research*, 49(20), 2415-2441, https://doi.org/10.1016/j.visres.2009.08.010.

Rucci, M., & Victor, J. D. (2015). The unsteady eye: an information-processing stage, not a bug. *Trends in neurosciences*, 38(4), 195-206, https://doi.org/10.1016/j.tins.2015.01.005.

Schor, C. M., & Ciuffreda, K. J. (1983). Accommodative Vergence and Accommodation in Normals, Amblyopes, and Strabismics. *Vergence Eye Movements: Basic*, 143.

Sheehy, C. K., Yang, Q., Arathorn, D. W., Tiruveedhula, P., de Boer, J. F., & Roorda, A. (2012). High-speed, image-based eye tracking with a scanning laser ophthalmoscope. *Biomedical optics express*, 3(10), 2611-2622, https://doi.org/10.1364/BOE.3.002611.

Shenoy, J., Fong, J., Tan, J., Roorda, A., & Ng, R. (2021). R-SLAM: Optimizing Eye Tracking from Rolling

Shutter Video of the Retina. *In Proceedings of the IEEE/CVF International Conference on Computer Vision* (pp. 4852-4861).

Simon, F., Schulz, E., Rassow, B., & Haase, W. (1984). Binocular micromovement recording of human eyes: - methods. *Graefe's archive for clinical and experimental ophthalmology*, 221(6), 293-298., https://doi.org/10.1007/BF02134127.

Spauschus, A., Marsden, J., Halliday, D. M., Rosenberg, J. R., & Brown, P. (1999). The origin of ocular microtremor in man. *Experimental Brain Research*, 126(4), 556-562, https://doi.org/10.1007/s002210050764.

Steinman, S. B., Steinman, B. A., & Garzia, R. P. (2000). Foundations of binocular vision: a clinical perspective. *McGraw-Hill Education/Medical.*

Steven, S., Sulai, Y. N., Cheong, S. K., Bentley, J., & Dubra, A. (2018). Long eye relief fundus camera and fixation target with partial correction of ocular longitudinal chromatic aberration. *Biomedical Optics Express*, 9(12), 6017-6037, https://doi.org/10.1364/BOE.9.006017.

Stevenson, S. B., Roorda, A., & Kumar, G. (2010). Eye tracking with the adaptive optics scanning laser ophthalmoscope. *In Proceedings of the 2010 symposium on eye-tracking research & applications* (pp. 195-198), https://doi.org/10.1145/1743666.1743714.

Stevenson, S. B., Sheehy, C. K., & Roorda, A. (2016). Binocular eye tracking with the tracking scanning laser ophthalmoscope. *Vision research*, 118, 98-104, https://doi.org/10.1016/j.visres.2015.01.019.

Szkulmowski, M., Meina, M., Bartuzel, M., Wrobel, K., Tamborski, S., Nowakowski, M. & Szkulmowska, A. (2020). Ultrafast retinal tracker for quantification of fixational and saccadic motion of the human eye. *Investigative Ophthalmology & Visual Science*, *61*(7), 1849-1849.

Tweed, D. (1997). Visual-motor optimization in binocular control. *Vision research*, 37(14), 1939-1951, https://doi.org/10.1016/S0042-6989(97)00002-3.

Van Rijn, L. J., Van der Steen, J., & Collewijn, H. (1992). Visually induced cycloversion and cyclovergence. *Vision Research*, 32(10), 1875-1883, https://doi.org/10.1016/0042-6989(92)90048-N.

Van Rijn, L. J., Van der Steen, J., & Collewijn, H. (1994). Instability of ocular torsion during fixation: cyclovergence is more stable than cycloversion. *Vision Research*, *34*(8), 1077-1087, https://doi.org/10.1016/0042-6989(94)90011-6.

Vogel, C. R., Arathorn, D. W., Roorda, A., & Parker, A. (2006). Retinal motion estimation in adaptive optics scanning laser ophthalmoscopy. *Optics express*, 14(2), 487-497, https://doi.org/10.1364/OPEX.14.000487.

Zhou, W., & King, W. M. (1998). Premotor commands encode monocular eye movements. *Nature*, 393(6686), 692-695, https://doi.org/10.1038/31489.